



Porous Materials Hot Paper

How to cite: *Angew. Chem. Int. Ed.* **2021**, *60*, 17455–17463

International Edition: doi.org/10.1002/anie.202102982

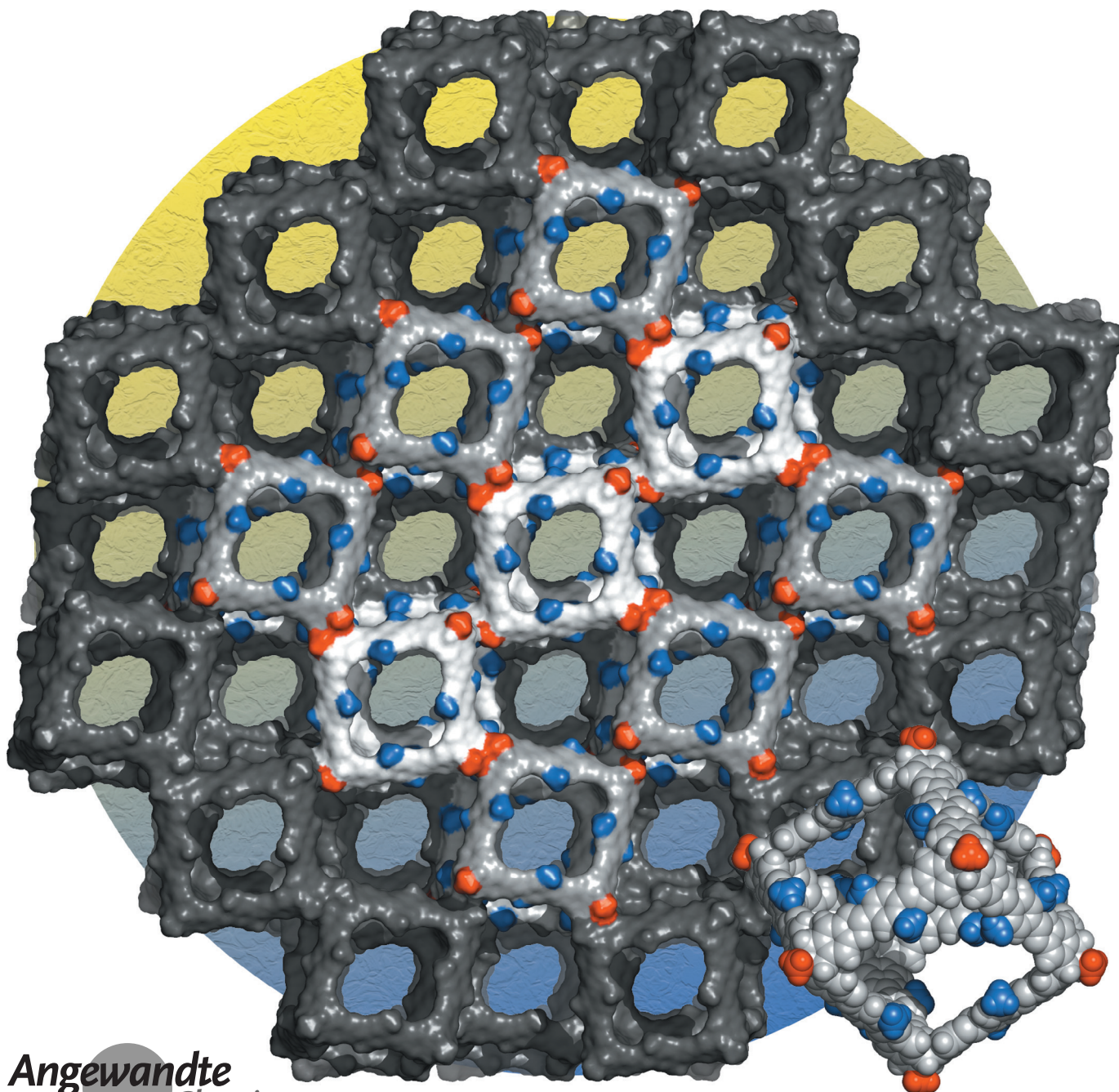
German Edition: doi.org/10.1002/ange.202102982



Isorecticular Crystallization of Highly Porous Cubic Covalent Organic Cage Compounds**

*Svetlana Ivanova, Eva Köster, Julian J. Holstein, Niklas Keller, Guido H. Clever, Thomas Bein, and Florian Beuerle**

In memory of Professor Siegfried Hünig



Angewandte
International Edition
Chemie

Abstract: Modular frameworks featuring well-defined pore structures in microscale domains establish tailor-made porous materials. For open molecular solids however, maintaining long-range order after desolvation is inherently challenging, since packing is usually governed by only a few supramolecular interactions. Here we report on two series of nanocubes obtained by co-condensation of two different hexahydroxy tribenzotriquinacenes (TBTQs) and benzene-1,4-diboronic acids (BDBAs) with varying linear alkyl chains in 2,5-position. *n*-Butyl groups at the apical position of the TBTQ vertices yielded soluble model compounds, which were analyzed by mass spectrometry and NMR spectroscopy. In contrast, methyl-substituted cages spontaneously crystallized as isostructural and highly porous solids with BET surface areas and pore volumes of up to $3426\text{ m}^2\text{ g}^{-1}$ and $1.84\text{ cm}^3\text{ g}^{-1}$. Single crystal X-ray diffraction and sorption measurements revealed an intricate cubic arrangement of alternating micro- and mesopores in the range of $0.97\text{--}2.2\text{ nm}$ that are fine-tuned by the alkyl substituents at the BDBA linker.

Introduction

Reticular chemistry assembles open crystalline frameworks by linking rigid molecular building blocks through strong covalent bonds.^[1] Metal–organic frameworks (MOFs)^[2] and covalent organic frameworks (COFs)^[3] are the most developed classes of such porous materials^[4] with the prospect of applications in gas storage^[5] and separation,^[6] membranes^[7] or sensing.^[8] Since crystal lattice energies are dominated by the directional covalent or coordinating coupling interactions,^[9] isorecticular frameworks are accessible via the formal exchange of structurally similar building blocks.^[10] Thereby, materials properties can be fine-tuned while still maintaining the underlying topology and superstructure.

In the last two decades, porous molecular materials,^[9,11] e.g., organic cages^[3d,12] or molecules of intrinsic microporosity (MIMs),^[13] which could be arranged by hydrogen bonding^[14] or ionic interactions,^[15] have emerged as alternatives for polymeric frameworks. Utilizing dynamic covalent chemistry,^[16] a steadily growing number of imine,^[17] boronate ester^[18] (Figure 1), boroxine^[19] or alkyne^[20] cages is now accessible. Whereas the molecular character of cages was exploited for host–guest chemistry,^[21] self-sorting,^[22] mechanical interlock-

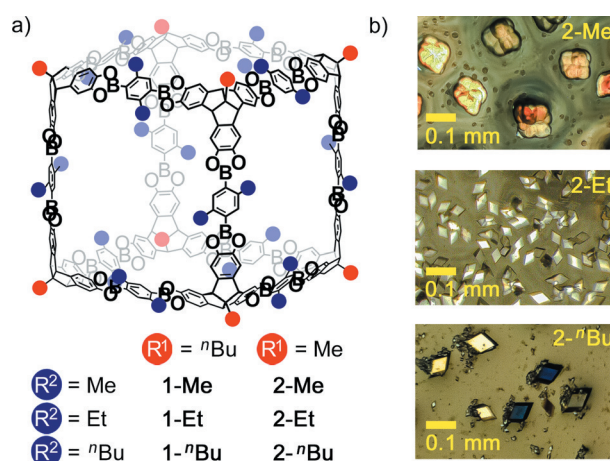


Figure 1. a) Chemical structure and substituents for cubic cages 1 and 2 and b) optical microscopy images of crystalline samples for cages 2.

ing^[23] or reactivity control for encapsulated guests,^[24] these “soluble porous units”^[25] could also be processed into mixed-matrix membranes^[26] or as active components in sensing devices.^[27] However, the design of crystalline cage materials with defined pore systems following basic geometrical principles is still highly challenging.^[9,28] Since the lattice energy is rarely dominated by a single directional intermolecular motif, even subtle structural modifications at the molecular modules, e.g., inversion of chiral elements,^[22g] frequently alter crystal packing, thus preventing isostructural crystallization even for structurally very similar cages.^[17b,29]

So far, isorecticular series of porous organic cage crystals have only been achieved with the help of additional design strategies such as computational crystal structure prediction,^[30] chiral recognition^[31] or structure-directing guests.^[32] Sustaining both permanent porosity^[33] and precise structural order^[34] after solvent removal or in bulk samples remains a nontrivial task and BET surface areas SA_{BET} surpassing $1000\text{ m}^2\text{ g}^{-1}$ have only been reported for a few cases.^[17a,20,22g,23b,32a,35] Reaching even higher values of $SA_{\text{BET}} > 2000\text{ m}^2\text{ g}^{-1}$ ^[17b,31e,36] and pore volumes $V_{\text{pore}} > 1\text{ cm}^3\text{ g}^{-1}$ proved extremely difficult and a cuboctahedral boronate ester cage reported in 2014 by the Mastalerz group still remains the benchmark for both figures of merit with $SA_{\text{BET}} = 3758\text{ m}^2\text{ g}^{-1}$ and $V_{\text{pore}} = 1.41\text{ cm}^3\text{ g}^{-1}$.^[18c]

[*] S. Ivanova, E. Köster, Priv.-Doz. Dr. F. Beuerle
Julius-Maximilians-Universität Würzburg
Institut für Organische Chemie
Am Hubland, 97074 Würzburg (Germany)
E-mail: florian.beuerle@uni-wuerzburg.de

S. Ivanova, E. Köster, Priv.-Doz. Dr. F. Beuerle
Julius-Maximilians-Universität Würzburg
Center for Nanosystems Chemistry (CNC)
Theodor-Boveri-Weg, 97074 Würzburg (Germany)

Dr. J. J. Holstein, Prof. Dr. G. H. Clever
Technische Universität Dortmund
Fakultät für Chemie und Chemische Biologie
Otto-Hahn-Strasse 6, 44227 Dortmund (Germany)

Dr. N. Keller, Prof. Dr. T. Bein
Ludwig-Maximilians-Universität München
Department of Chemistry & Center for NanoScience (CeNS)
Butenandtstrasse 5–13, 81377 München (Germany)

[**] A previous version of this manuscript has been deposited on a preprint server (<https://doi.org/10.26434/chemrxiv.14132108>).

Supporting information and the ORCID identification number(s) for the author(s) of this article can be found under:
<https://doi.org/10.1002/anie.202102982>.

© 2021 The Authors. Angewandte Chemie International Edition published by Wiley-VCH GmbH. This is an open access article under the terms of the Creative Commons Attribution Non-Commercial NoDerivs License, which permits use and distribution in any medium, provided the original work is properly cited, the use is non-commercial and no modifications or adaptations are made.

Here we report on the synthesis of two series of cubic covalent organic cage compounds **1** and **2** (Figure 1 a) by the co-condensation of two different hexahydroxy tribenzotriquinacenes (TBTQs)^[37] with benzene-1,4-diboronic acids (BDBAs) possessing alkyl chains of varying length in 2,5-position. ⁿBu groups at the apical position of the TBTQs yielded soluble model compounds **1**, which were analyzed by ¹H, ¹³C, diffusion ordered (DOSY) NMR spectroscopy and mass spectrometry. The respective Me-substituted cages **2**, however, crystallized directly from the reaction solutions in an isorecticular fashion (Figure 1 b) and were characterized by single-crystal X-ray diffraction (SC-XRD) and BET sorption measurements.

Results and Discussion

In previous work,^[18a] we synthesized molecular nanocubes through the [8+12] co-condensation of orthogonal TBTQs and linear BDBAs. The introduction of ⁿBu chains at the apical position (red in Figure 1 a) of **TBTQ-ⁿBu** in cages **1** assured sufficient solubility during the assembly process, with **1-H** and **1-ⁿBu** being isolated as precipitate and in solution, respectively. At that time, the synthesis of **2-H** with Me substituents at the TBTQs and unfunctionalized BDBA linkers failed due to immediate precipitation of early cage intermediates.

To further probe the effect of varying alkyl substituents on the subtle balance between solubility and precipitation, we synthesized **BDBA-Me**^[38] and **BDBA-Et** bearing Me or Et groups at the 2,5-positions (blue in Figure 1). As expected, novel cubic cages **1-Me** and **1-Et** self-assembled from THF solutions of **TBTQ-ⁿBu** and **BDBA-X** (X = Me or Et) at 2:3 ratio after repeated addition of 4 Å molecular sieves over five days (see SI for experimental and analytical details). Thus, a series of cages **1** was established in which the solubility in organic solvents gradually decreased with shorter alkyl chains at the edges. The solubility of cages **1-ⁿBu** and **1-Et** in CHCl₃ was high enough to allow characterization by MALDI-TOF MS (Figure S12), ¹H and ¹³C NMR spectroscopy (Figures S6–S7). For cage **1-Me** however, only MALDI-TOF MS was measurable from CHCl₃ solution (Figure S11), whereas ¹H NMR had to be recorded in C₂D₂Cl₄ (Figure S5). As expected, all three cages **1** showed only two aromatic singlets at around 8.0 and 7.4 ppm (Figure 2) for the BDBA and TBTQ moieties, respectively, and one singlet at 4.6 ppm for the bridgehead protons at the TBTQ vertices, thus indicating the formation of cubic cages with O_h symmetry. As reported previously,^[18a] cage **1-H** proved insoluble in common organic solvents and precipitated directly from the reaction mixture. However, cage formation was detected by MALDI-TOF MS after trituration with solid matrix.

To probe the size and mobility of cubic cages **1** in solution, diffusion coefficients of 7.67×10^{-11} , 2.29×10^{-10} and 2.20×10^{-10} m²s⁻¹ for cages **1-Me**, **1-Et** and **1-ⁿBu**, respectively, were obtained by DOSY NMR (Figure 2). To compare values obtained from different solvents (C₂D₂Cl₄ for **1-Me**, CDCl₃ for **1-Et** and **1-ⁿBu**), solvodynamic diameters were calculated via the Stokes–Einstein equation (see Tables S1, S2 and

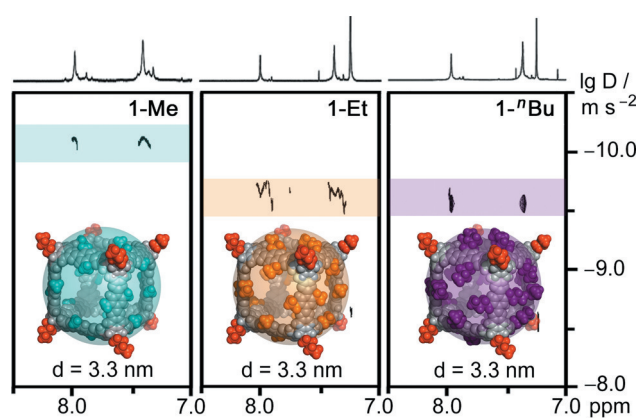


Figure 2. DOSY NMR spectra (600 MHz, C₂D₂Cl₄ or CDCl₃, rt) for cages **1** (solvodynamic diameters are indicated as transparent spheres in the PM6-minimized^[39] space-filling models, images have been prepared with PyMOL^[40]).

Figures S16–S21 for details). Strikingly, identical diameters of 3.3 nm were obtained for all cages **1**. Apparently, the increasing length of the alkyl chains at the BDBA edges hardly influences the mobility in solution, which is merely determined by the size and shape of the rigid cubic backbone. As indicated by the PM6^[39]-models in Figure 2, these substituents might however modulate the size of the pore windows. Further investigations regarding cages with other rigid or flexible substituents will give more insight into the relation between diffusion properties and molecular structure and are currently underway in our laboratories.

Despite numerous attempts so far, no single crystals suitable for X-ray diffraction (SC-XRD) could be obtained for cages **1**. Apparently, the exposed ⁿBu substituents at the TBTQs prevent efficient packing due to considerable steric demand at the cube vertices (Figure 3 a, top). Recently, Mastalerz and co-workers reported impressive SC-XRD structures for chiral imine cages^[22g] based on a TBTQ derivative with Me and ⁿPr substituents at the apical and bridgehead positions, respectively. In the solid state, these cages were held together by weak and unspecific van der Waals forces between the ⁿPr chains of neighboring cages. Due to rotations at the more flexible imine linkages, the shape of the cages also slightly deviated from perfect cubes. Therefore, different packing modes were observed for two diastereomeric cages and partial structural collapse after desolvation occurred. For more rigid boronate ester cages, we expected cages **2** based on **TBTQ-Me** to possess a more rigid and cubic geometry, thus anticipating a more efficient packing in the solid state (Figure 3 a, bottom). In addition, stronger supramolecular interactions between the π systems of the BDBA edges should strengthen the intramolecular forces between individual cages, thus stabilizing and rigidifying the solid-state packing. As we previously failed to assemble **2-H**,^[18a] we modulated the solubility of cages **2** by attaching alkyl substituents at the BDBA linkers.

Following our established protocol,^[18a] **TBTQ-Me** and **BDBA-X** (X = Me, Et or ⁿBu) at 2:3 ratio were dissolved in [D₈]THF at room temperature and 4 Å molecular sieves were added. Monitoring of the reaction progress by ¹H NMR

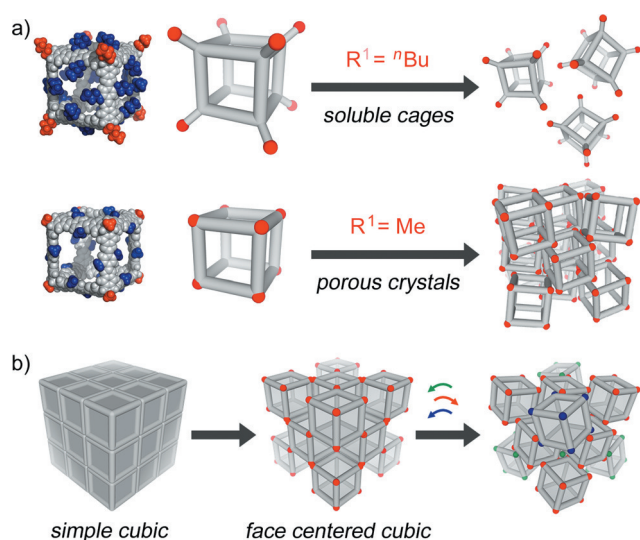


Figure 3. a) Control over solubility or crystallinity of cubic cages depending on substituents R^1 at the TBTQ vertices and b) schematic packing motifs for hollow cubic cages.

revealed a fast decrease in signal intensity and crystalline precipitates occurred after one day. The very low concentrations in the remaining solutions and the fact that the reaction products could not be redissolved without decomposition prevented analysis by NMR spectroscopy. However, MALDI-TOF MS of both the supernatant solutions and precipitates showed cages **2** as the only detectable products (Figures S13–S15).

Optical microscopy images (Figure 1b) revealed similar diamond-shaped crystals for **2-Et** and **2-nBu**. For **2-Me**, smaller and more intergrown crystallites were obtained due to lower solubility and thus, faster crystal growth. For all three cages, we could isolate single crystals of decent shape and size. However, the highly porous structures contain very large amounts of solvent ranging from 69% to 77%. Due to the extremely weak diffraction power, synchrotron radiation was required for structure elucidation.^[41] Utilizing macromolecular beamline P11, DESY (Hamburg)^[42] at a chosen wavelength in between 0.77 and 0.98 Å allowed us to push the experimental resolution into the 1.3–1.4 Å regime, which is just sufficient for ab initio structure solution with SHELXT.^[43] For **2-Me** and **2-Et**, the cage model could be fully completed in the subsequent refinement, but only one of the four n Bu side chains in the asymmetric unit of **2-nBu** could be located in the observed electron density map. It was found to be

disordered over two conformations. At the other three sites, there was not enough electron density to locate the orientation of the flexible n Bu substituents in full. In these three cases the side chains were modelled as methyl groups instead. The scattering contribution of unmodelled n Bu atoms and solvent molecules was treated with the SQUEEZE routine.^[44] With cube diameters of 3.4 nm (Table S4) these nanocubes rank among the largest purely organic cages that have been analyzed by SC-XRD so far. The cuboctahedral^[18c] and cubic^[22g] cages from the Mastalerz group are roughly the same size and are only surpassed by the giant porphyrin boxes^[17d] from the Kim group.

Remarkably, all cages **2** crystallized in the same trigonal space group $R\bar{3}c$ with nearly identical unit cell dimensions (Table 1). Both individual cages (Figure 4a) and unit cells (Figure 4b) almost perfectly superimpose, thus emphasizing the isoreticular packing within the series of cages **2**. Owing to the rigid and directional boronate ester linkages, all cage monomers show only slight deviations from a perfect cubic geometry (Table S4). For one of the two BDBA linkers in the asymmetric unit, the alkyl substituents are statistically disordered (Figure S25d) by rotation around the edges, whereas the alkyl groups for the second BDBA unit assist in stabilizing the packing and are therefore fixed in one conformation (Figures 4e and S25c). As anticipated, individual cages are linked via π – π interactions between the BDBA struts and there is almost no influence of the alkyl substituents on the solid-state packing. Thus, the general packing motif can be deduced from a simple model of a cube as the only space-filling Platonic solid (Figure 3b, left). Since cages **2** possess empty windows at the faces, stabilizing interactions can only arise between the π surfaces of the aromatic edges. Removal of every second cage from the simple cubic lattice gives a face-centered cubic (fcc) arrangement (Figure 3b, middle) facilitating π stacking between pairs of edges. Still, four vertices collide at the specific lattice points (Figure 3b, red dots). Alternate clock- and anticlockwise rotation of 15° for all cages within consecutive hexagonal layers evades this steric pressure (Figure 3b, right), thus leading to the pseudo fcc packing, which will be now discussed at the example of **2-Me**.

Two different types of π – π interactions, for the inter-(rose/blue in Figure 4c) or intralayer (rose/rose in Figure 4c) contacts of adjacent cages, account for the lattice energy of the structure. Caused by the alternating rotation of every second hexagonal layer (Figure 4e), the unit cell is doubled along the c axis and the layers are arranged in an AB'CA'BC'

Table 1: Crystallographic parameters and gas sorption properties of crystalline cages **2**.

Cage	space group	α, β [°]	γ [°]	a, b [Å]	c [Å]	SASA ^[a] [m ² g ⁻¹]	SA _{BET} ^[c] [m ² g ⁻¹]	free volume ^[d] [cm ³ g ⁻¹]	V_{pore} ^[e] [cm ³ g ⁻¹]	pore A ^[f] (intrinsic) [nm]	pore B ^[f] (window) [nm]	pore C ^[f] (extrinsic) [nm]
2-Me	$R\bar{3}c$	90	120	31.821	135.777	3727	2722	2.01 (77%)	1.01	1.10	1.48	2.27
2-Et	$R\bar{3}c$	90	120	31.659	136.496	3759	2531	1.79 (74%)	1.28	1.01	1.42	2.19
2-nBu	$R\bar{3}c$	90	120	31.683	137.915	3839 ^[b]	3426	1.49 (69%)	1.84	0.97	1.36	2.19

[a] Solvent-accessible surface area (SASA) calculated for the SC-XRD structure with Materials Studio (N_2 -sized probe with $R = 1.84$ Å, 0.25 Å grid interval with fine resolution).^[46] [b] SASA calculated for the SC-XRD structure with manually added n Bu chains with Materials Studio.^[46] [c] BET surface area for N_2 at 77 K. [d] Calculated for the Connolly surface ($R = 1.84$ Å) with Materials Studio^[46] (free volume proportion of the unit cell is given in brackets). [e] Calculated from sorption measurements. [f] Calculated with a quenched solid DFT (QSDF) carbon kernel for slit and cylindrical pores.

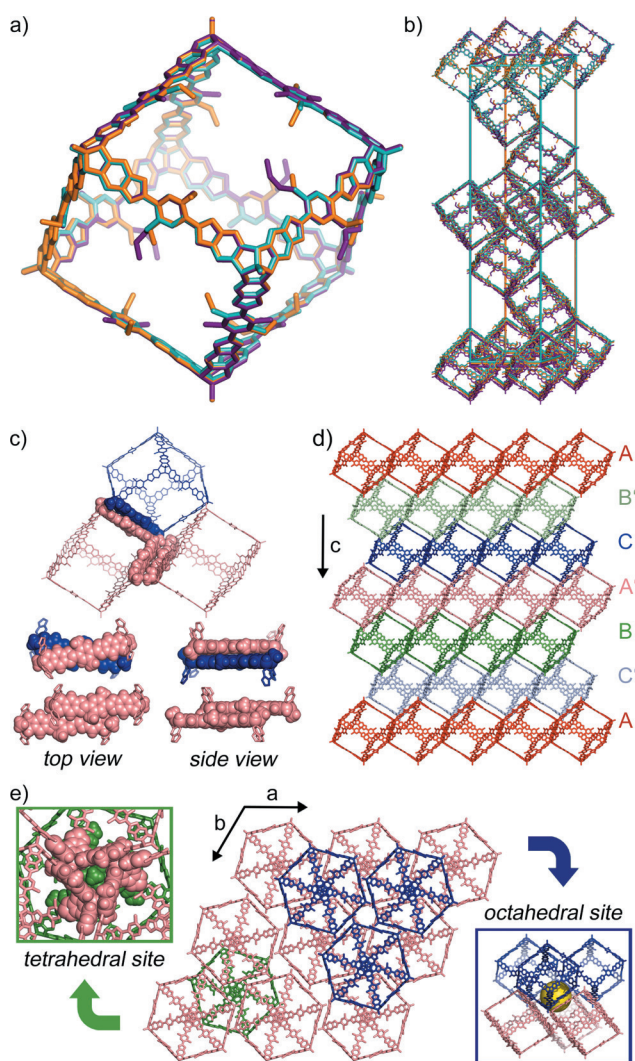


Figure 4. Overlay of a) monomers and b) unit cells for SC-XRD structures of cages **2-Me** (turquoise), **2-Et** (orange) and **2-ⁿBu** (violet); fcc packing for **2-Me**: c) two types of π - π interactions between BDDBA edges (rose/blue for interlayer and rose/rose for intralayer interactions), d) AB'CA'BC'-type layer stacking and e) top view for hexagonal layers (insets show the Me pockets at the tetrahedral sites (green box) and the extrinsic pore (yellow) at the octahedral sites (blue box), all images have been prepared with PyMOL^[40]).

stacking (Figure 4 d). At the tetrahedral sites, the synchronous rotations within one layer open small cavities that provide an exact fit for the apical Me groups from the neighboring layers (green box in Figure 4 e). These Me- π interactions nicely illustrate the crucial role of the apical Me groups, as any larger substituent would not fit, and thus, prevent this type of packing. Each octahedral site defines one extrinsic pore which is surrounded by six cages (blue box in Figure 4 e) in a face-to-face fashion. Overall, the alternating arrangement of intrinsic and extrinsic pores (blue and yellow in Figure 5 d) creates a cubic pore system that is continuous in all three spatial directions (Figure 5 b).

To probe the structural integrity and permanent porosity of cages **2**, crystalline bulk samples were isolated after five days in 55–66% yield. Work-up included isolation of the

crude crystalline material, washing with CHCl_3 and immediate transfer to *n*-pentane for solvent exchange (5×24 hours). Once submerged in *n*-pentane, cage materials proved stable over several weeks as evidenced by powder X-ray diffraction (PXRD). Thermogravimetric analysis (TGA) of solid samples after solvent exchange revealed slight weight losses of 5–10% up to 200 °C, which presumably correspond to the removal of residual solvents from the pores, followed by decomposition starting at around 400 °C. The comparison of PXRD data for bulk samples of cages **2** with diffractograms simulated from the SC-XRD structures revealed the structural integrity for this isoreticular series of porous cages. The good match between experimental and simulated diffractograms (Figures 5 a and S31–S33) indicated the formation of extended bulk domains resembling the single crystal structure. All measured diffractograms are dominated by one very intense reflection at around 4° which corresponds to the {104} planes (Figure 5 a) and represents the cube-to-cube spacing within the fcc packing (Figure 5 b).

Minor deviations in 2θ values are presumably caused by slight shifts or rotations of the individual cages after solvent removal or different temperatures for the single-crystal and powder measurements. Nevertheless, the rather strong and directional π - π interactions (Figure 4 c) between the cages stabilize the packing arrangement in desolvated samples, which is rarely observed for organic cages of such size.^[3d,11] The unique cubic shapes of cages **2** establish these materials as supramolecular analogs of 3D COFs that maintain a defined 3D pore structure after activation, thus allowing for a tailor-made design of porous materials. To assess permanent porosity, we measured N_2 sorption at 77 K for activated cage powders. The obtained isotherms (Figure 5 c) are best described as type I(b) isotherms indicating the presence of micro- and mesopores with pore sizes below 2.5 nm.^[45] After applying Brunauer-Emmett-Teller (BET) theory, SA_{BET} values of 2722, 2531 and 3426 $\text{m}^2 \text{g}^{-1}$ (Table 1) were obtained for **2-Me**, **2-Et** and **2-ⁿBu**, respectively. Thus, all crystals **2** are among the very few examples with $\text{SA}_{\text{BET}} > 2500 \text{m}^2 \text{g}^{-1}$ reported so far.^[33b,36] Within this isoreticular series, **2-ⁿBu** exhibits the highest surface area, reaching 89% of the solvent-accessible surface area (SASA) of 3839 $\text{m}^2 \text{g}^{-1}$, which was calculated from the SC-XRD structure with Materials Studio^[46] for a N_2 -sized probe with $R = 1.84 \text{Å}$ (see Table 1). However, this SASA, being a theoretical limit, should be treated with caution, as 18 of the 24 ⁿBu chains have not been resolved in the SC-XRD structure but were only added manually to this model. It is also not yet understood how these flexible substituents protruding into the extrinsic pores contribute to the surface area. For **2-Me**, lower solubility leads to faster nucleation and, thus, precipitation of smaller and less regular crystals. For **2-Et** and **2-ⁿBu**, similarly looking crystalline samples were isolated (Figure 1 b). However, bulk samples of **2-Et** appeared to be more sensitive during the solvent exchange. For **2-Me** and **2-Et**, SA_{BET} values ranging from 1200 to 2700 $\text{m}^2 \text{g}^{-1}$ were obtained for slightly different activation procedures. In particular, fast transfer from THF to *n*-pentane proved to be crucial for high porosity. At the moment, we attribute the differences in SA_{BET} to varying amounts and size of highly porous domains in the active

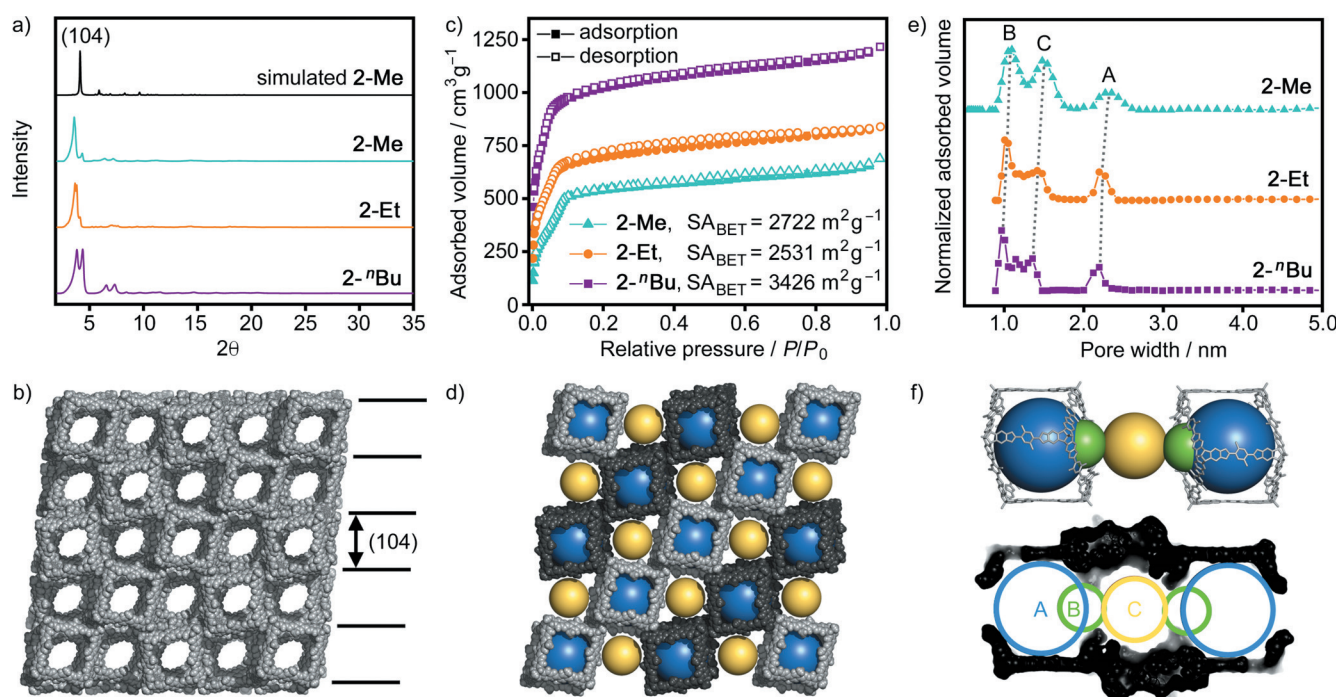


Figure 5. a) Powder X-ray diffractograms simulated from single-crystal data for **2-Me** (black) and for bulk materials of cages **2**; b) space-filling model of the porous structure of **2-Me** indicating the (104) lattices planes; c) N_2 sorption isotherms for cages **2** at 77 K (filled and open symbols represent adsorption and desorption branches, respectively); d) 2D view of the alternating arrangement of intrinsic (blue) and extrinsic (yellow) pores (cages from adjacent hexagonal layers are indicated in light and dark gray); e) pore size distributions calculated by quenched solid DFT for cages **2** and f) detailed visualization (top) and thin section slice (bottom) for linear array of intrinsic (A, blue) and extrinsic (C, yellow) pores connected by cage windows (B, green) along the channels of **2-Me**.

materials.^[12c,22g] However, more studies are needed in the future to fully elucidate the peculiar effects of R^2 substituents on the porosity. Cage-based crystals **2-Me**, **2-Et** and **2-nBu** also feature exceptionally large V_{pore} of 1.01, 1.28 and 1.84 $\text{cm}^3 \text{g}^{-1}$, respectively. Obtaining V_{pore} values larger than 1 $\text{cm}^3 \text{g}^{-1}$ is extremely rare for organic cages and, to the best of our knowledge, **2-nBu** exhibits the highest value for this class of materials reported so far.^[12c]

Pore size distributions (PSD) were calculated from the adsorption branch of the N_2 isotherms using a quenched solid DFT (QSDFT) carbon kernel for slit and cylindrical pores. Intriguingly, three well-defined and narrow pore sizes were identified for all three cage-based crystals **2** at the boundary of the micro- and mesopore regimes between 0.97 and 2.3 nm (Table 1 and Figure 5e). Hence, cages **2** are among the very few organic cages exhibiting both micro- and mesoporosity within the same porous material.^[23b] We attribute mesopores A to the intrinsic cage cavities (blue in Figure 5f), since the pore size of 2.2–2.3 nm fits very well to the distance of approximately 2.3 nm between diagonal edges in the SC-XRD structures (see Table S4 for exact values). Furthermore, the two micropores B (ca. 1.0 nm) and C (ca. 1.5 nm) are best assigned to the cage windows and extrinsic pores, respectively (green and yellow in Figure 5f).

The thin section image for a short channel fragment consisting of two cages that are connected by one extrinsic pore in Figure 5f nicely illustrates the remarkable correlation of the DFT-derived pore sizes with the structural model. Whereas pores A and B, which are intrinsically related to the

cavity and windows of the rigid cubic cages, show a very narrow distribution, extrinsic pores C appear somewhat broader in the PSD calculations. We attribute this effect to the much higher susceptibility of the extrinsic pores towards small shifts and rotations in the packing arrangement. As mentioned earlier, PXRD data also indicated minor movements in the supramolecular packing. Nevertheless, these combined data still support the essential integrity of well-defined channels of alternating micro- and mesopores along all three spatial directions even in the desolvated state (Figure 5b,d).

Whereas the isostructural crystallization establishes identical 3D pore systems for all cages **2**, the pore sizes are however subtly tuned by the different substituents at the BDBA linkers (Figures 5e,f and 6). As expected, the intrinsic cavities A are hardly affected by the dangling alkyl chains at the edges. Instead, these groups are predominantly located in the extrinsic voids or partially block the cage windows, thus reducing the size of micropores B and C with increasing chain length (Table 1 and Figure S37 for thin section images). Figure 6 illustrates the overall effect on the channel diameter and the aperture of the square windows for the cubic cages. For further visualization, videos for a thin section side view of the rotation around the channel axis for all cages **2** are available in the SI.

This observation is quite appealing as it might just provide the control over the pore system that is needed to combine high selectivity with large storage capacity. Just recently, the combination of barely porous imine cages with larger storage

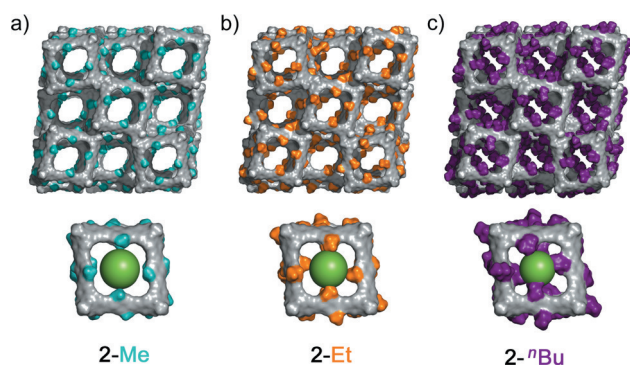


Figure 6. Front view for a 3×3 array of parallel porous channels (top) and enlarged view of one specific pore window (bottom, QSDFT-derived pore size indicated as green sphere in the middle of the window) for a) **2-Me**, b) **2-Et** and c) **2-nBu** (Connolly surface is shown for all cages, nBu side chains that could not be resolved crystallographically have been added manually in Materials Studio;^[46] images have been prepared with PyMOL^[40]).

pores proved to be highly selective for the separation of hydrogen isotopes.^[47] In particular, the alternating arrangement of two pores with different sizes throughout the structure induced an additional sieving effect, as faster diffusing absorbents can pass while crossing the larger pores.

Similar effects are conceivable for cages **2** and novel derivatives thereof, as the attachment of recognition sites at the BDBA units could lead to tailor-made selection pores in combination with very high uptake capacity for the intrinsic mesopores. Currently, we are exploring the potential of cages **2** for selective gas sorption and for developing the next generation of cubic cages to further improve the porous properties of molecular materials.

Conclusion

Two series of covalent organic nanocubes **1** and **2** with varying alkyl substituents at both the hexahydroxy TBTO vertices and BDBA edges have been synthesized. nBu functionalization at the apical position of the TBTO corners yielded soluble cages **1** as model compounds for crystalline cages **2** with Me functionalization. Cages **1** were characterized by common solution techniques such as NMR spectroscopy or mass spectrometry. Alkyl functionalization at the BDBA linkers modulated the size of the square pore windows but did not influence size and diffusion of molecular cages in solution as evidenced by identical solvodynamic diameters of 3.3 nm calculated from DOSY measurements. Cages **2** crystallized in an isorecticular fashion with an fcc packing mode regardless of the different side chains at the BDBA linkers. Bulk samples were analyzed by sorption measurements revealing very high BET surface areas of up to $3426 \text{ m}^2 \text{ g}^{-1}$ and exceptionally high pore volumes of up to $1.84 \text{ cm}^3 \text{ g}^{-1}$. These values are among the highest reported for covalent organic cage compounds so far. Crystalline samples exhibited high structural stability and the isorecticular packing motif provided facile and predictable access to 3D connected pore systems, thus tackling two very important challenges for molecular porous materials. QSDFT

pore size distributions revealed three different pore sizes at around 1.0, 1.5 and 2.2 nm for all cages **2**, which are assigned to the cage windows, the extrinsic pores in the octahedral voids of the fcc packing, and the intrinsic cage cavities, respectively. Therefore, the series of porous materials **2** present a rare example for covalent organic cages with alternating micro- and mesopores within one material. Intriguingly, pore sizes are modulated by the alkyl substituents at the linear BDBA linkers. Specific functionalization will give access to tailor-made materials featuring designer pores with superior performance in selective sorption and gas separation. Further studies on cage derivatives with extended aromatic linkers and functional side chains will reveal the influence of such modifications on packing and porosity and are currently underway in our laboratories.

Acknowledgements

This work was financially supported by the DFG (BE4808/2-1) and the Collaborative Research Network “Solar Technologies Go Hybrid” of the Bavarian Ministry of Science, Research and the Arts. Diffraction data for single crystals of **2-Me**, **2-Et** and **2-nBu** was collected at PETRA III, DESY (Hamburg, Germany), a member of the Helmholtz Association (HGF). We thank Sofiane Saouane and Anja Burkhardt for assistance at synchrotron beamline P11 (I-20180990, I-20190495). We thank Lukas Hahn and Prof. Robert Luxenhofer for density and viscosity measurements as well as Julia Puck and Prof. Anke Krüger for TGA measurements. Open access funding enabled and organized by Projekt DEAL.

Conflict of interest

The authors declare no conflict of interest.

Keywords: boronate esters · cage compounds · dynamic covalent chemistry · porous materials · structure elucidation

- [1] a) O. M. Yaghi, M. O’Keeffe, N. W. Ockwig, H. K. Chae, M. Eddaoudi, J. Kim, *Nature* **2003**, *423*, 705–714; b) N. W. Ockwig, O. Delgado-Friedrichs, M. O’Keeffe, O. M. Yaghi, *Acc. Chem. Res.* **2005**, *38*, 176–182.
- [2] a) S. Kitagawa, R. Kitaura, S.-i. Noro, *Angew. Chem. Int. Ed.* **2004**, *43*, 2334–2375; *Angew. Chem.* **2004**, *116*, 2388–2430; b) *Metal-Organic Frameworks—Design and Application* (Ed.: L. R. MacGillivray), Wiley, Hoboken, **2010**; c) D. Farrusseng, *Metal-Organic Frameworks*, Wiley-VCH, Weinheim, **2011**.
- [3] a) A. P. Côté, A. I. Benin, N. W. Ockwig, M. O’Keeffe, A. J. Matzger, O. M. Yaghi, *Science* **2005**, *310*, 1166–1170; b) N. Huang, P. Wang, D. Jiang, *Nat. Rev. Mater.* **2016**, *1*, 16068; c) R. P. Bisbey, W. R. Dichtel, *ACS Cent. Sci.* **2017**, *3*, 533–543; d) F. Beuerle, B. Gole, *Angew. Chem. Int. Ed.* **2018**, *57*, 4850–4878; *Angew. Chem.* **2018**, *130*, 4942–4972; e) X. Chen, K. Geng, R. Liu, K. T. Tan, Y. Gong, Z. Li, S. Tao, Q. Jiang, D. Jiang, *Angew. Chem. Int. Ed.* **2020**, *59*, 5050–5091; *Angew. Chem.* **2020**, *132*, 5086–5129.

- [4] A. G. Slater, A. I. Cooper, *Science* **2015**, *348*, aaa8075.
- [5] a) R. E. Morris, P. S. Wheatley, *Angew. Chem. Int. Ed.* **2008**, *47*, 4966–4981; *Angew. Chem.* **2008**, *120*, 5044–5059; b) L. J. Murray, M. Dincă, J. R. Long, *Chem. Soc. Rev.* **2009**, *38*, 1294–1314.
- [6] a) J.-R. Li, J. Sculley, H.-C. Zhou, *Chem. Rev.* **2012**, *112*, 869–932; b) B. P. Biswal, A. Bhaskar, R. Banerjee, U. K. Kharul, *Nanoscale* **2015**, *7*, 7291–7298; c) B. P. Biswal, H. D. Chaudhari, R. Banerjee, U. K. Kharul, *Chem. Eur. J.* **2016**, *22*, 4695–4699; d) S. Huang, Y. Hu, L.-L. Tan, S. Wan, S. Yazdi, Y. Jin, W. Zhang, *ACS Appl. Mater. Interfaces* **2020**, *12*, 51517–51522.
- [7] a) A. Bétard, R. A. Fischer, *Chem. Rev.* **2012**, *112*, 1055–1083; b) J. Dechnik, J. Gascon, C. J. Doonan, C. Janiak, C. J. Sumbly, *Angew. Chem. Int. Ed.* **2017**, *56*, 9292–9310; *Angew. Chem.* **2017**, *129*, 9420–9439; c) S. Kandambeth, B. P. Biswal, H. D. Chaudhari, K. C. Rout, S. Kunjattu, S. Mitra, S. Karak, A. Das, R. Mukherjee, U. K. Kharul, R. Banerjee, *Adv. Mater.* **2017**, *29*, 1603945.
- [8] a) L. E. Kreno, K. Leong, O. K. Farha, M. Allendorf, R. P. Van Duyne, J. T. Hupp, *Chem. Rev.* **2012**, *112*, 1105–1125; b) Z. Hu, B. J. Deibert, J. Li, *Chem. Soc. Rev.* **2014**, *43*, 5815–5840; c) G. Das, B. P. Biswal, S. Kandambeth, V. Venkatesh, G. Kaur, M. Addicoat, T. Heine, S. Verma, R. Banerjee, *Chem. Sci.* **2015**, *6*, 3931–3939; d) K. Müller-Buschbaum, F. Beuerle, C. Feldmann, *Microporous Mesoporous Mater.* **2015**, *216*, 171–199.
- [9] M. A. Little, A. I. Cooper, *Adv. Funct. Mater.* **2020**, *30*, 1909842.
- [10] a) M. Eddaoudi, J. Kim, N. Rosi, D. Vodak, J. Wachter, M. O’Keeffe, O. M. Yaghi, *Science* **2002**, *295*, 469–472; b) A. P. Côté, H. M. El-Kaderi, H. Furukawa, J. R. Hunt, O. M. Yaghi, *J. Am. Chem. Soc.* **2007**, *129*, 12914–12915; c) D. Yuan, D. Zhao, D. Sun, H.-C. Zhou, *Angew. Chem. Int. Ed.* **2010**, *49*, 5357–5361; *Angew. Chem.* **2010**, *122*, 5485–5489; d) P. Pachfule, B. Garai, R. Banerjee, *Inorg. Chem.* **2016**, *55*, 7200–7205.
- [11] J. Tian, P. K. Thallapally, B. P. McGrail, *CrystEngComm* **2012**, *14*, 1909–1919.
- [12] a) M. Mastalerz, *Angew. Chem. Int. Ed.* **2010**, *49*, 5042–5053; *Angew. Chem.* **2010**, *122*, 5164–5175; b) G. Zhang, M. Mastalerz, *Chem. Soc. Rev.* **2014**, *43*, 1934–1947; c) T. Hasell, A. I. Cooper, *Nat. Rev. Mater.* **2016**, *1*, 16053; d) M. Mastalerz, *Acc. Chem. Res.* **2018**, *51*, 2411–2422; e) K. Acharyya, P. S. Mukherjee, *Angew. Chem. Int. Ed.* **2019**, *58*, 8640–8653; *Angew. Chem.* **2019**, *131*, 8732–8745.
- [13] a) P. Sozzani, A. Comotti, R. Simonutti, T. Meersmann, J. W. Logan, A. Pines, *Angew. Chem. Int. Ed.* **2000**, *39*, 2695–2699; *Angew. Chem.* **2000**, *112*, 2807–2810; b) P. Sozzani, S. Bracco, A. Comotti, L. Ferretti, R. Simonutti, *Angew. Chem. Int. Ed.* **2005**, *44*, 1816–1820; *Angew. Chem.* **2005**, *117*, 1850–1854; c) A. Comotti, S. Bracco, L. Ferretti, M. Mauri, R. Simonutti, P. Sozzani, *Chem. Commun.* **2007**, 350–352; d) R. G. D. Taylor, M. Carta, C. G. Bezzu, J. Walker, K. J. Msayib, B. M. Kariuki, N. B. McKeown, *Org. Lett.* **2014**, *16*, 1848–1851; e) R. G. D. Taylor, C. G. Bezzu, M. Carta, K. J. Msayib, J. Walker, R. Short, B. M. Kariuki, N. B. McKeown, *Chem. Eur. J.* **2016**, *22*, 2466–2472; f) N. B. McKeown, *Org. Mater.* **2020**, *2*, 20–25.
- [14] a) M. Mastalerz, I. M. Oppel, *Angew. Chem. Int. Ed.* **2012**, *51*, 5252–5255; *Angew. Chem.* **2012**, *124*, 5345–5348; b) I. Bassanetti, S. Bracco, A. Comotti, M. Negroni, C. Bezuidenhout, S. Canossa, P. P. Mazzeo, L. Marchió, P. Sozzani, *J. Mater. Chem. A* **2018**, *6*, 14231–14239.
- [15] G. Xing, I. Bassanetti, S. Bracco, M. Negroni, C. Bezuidenhout, T. Ben, P. Sozzani, A. Comotti, *Chem. Sci.* **2019**, *10*, 730–736.
- [16] Y. Jin, C. Yu, R. J. Denman, W. Zhang, *Chem. Soc. Rev.* **2013**, *42*, 6634–6654.
- [17] a) M. Mastalerz, M. W. Schneider, I. M. Oppel, O. Presly, *Angew. Chem. Int. Ed.* **2011**, *50*, 1046–1051; *Angew. Chem.* **2011**, *123*, 1078–1083; b) M. W. Schneider, I. M. Oppel, H. Ott, L. G. Lechner, H.-J. S. Hauswald, R. Stoll, M. Mastalerz, *Chem. Eur. J.* **2012**, *18*, 836–847; c) S. Bera, K. Dey, T. K. Pal, A. Halder, S. Tothadi, S. Karak, M. Addicoat, R. Banerjee, *Angew. Chem. Int. Ed.* **2019**, *58*, 4243–4247; *Angew. Chem.* **2019**, *131*, 4287–4291; d) J. Koo, I. Kim, Y. Kim, D. Cho, I.-C. Hwang, R. D. Mukhopadhyay, H. Song, Y. H. Ko, A. Dhamija, H. Lee, W. Hwang, S. Kim, M.-H. Baik, K. Kim, *Chem* **2020**, *6*, 3374–3384; e) L. Zhang, Y. Jin, G.-H. Tao, Y. Gong, Y. Hu, L. He, W. Zhang, *Angew. Chem. Int. Ed.* **2020**, *59*, 20846–20851; *Angew. Chem.* **2020**, *132*, 21032–21037.
- [18] a) S. Klotzbach, T. Scherpf, F. Beuerle, *Chem. Commun.* **2014**, *50*, 12454–12457; b) S. Klotzbach, F. Beuerle, *Angew. Chem. Int. Ed.* **2015**, *54*, 10356–10360; *Angew. Chem.* **2015**, *127*, 10497–10502; c) G. Zhang, O. Presly, F. White, I. M. Oppel, M. Mastalerz, *Angew. Chem. Int. Ed.* **2014**, *53*, 1516–1520; *Angew. Chem.* **2014**, *126*, 1542–1546; d) S. M. Elbert, N. I. Regenauer, D. Schindler, W. S. Zhang, F. Rominger, R. R. Schröder, M. Mastalerz, *Chem. Eur. J.* **2018**, *24*, 11438–11443.
- [19] K. Ono, K. Johmoto, N. Yasuda, H. Uekusa, S. Fujii, M. Kiguchi, N. Iwasawa, *J. Am. Chem. Soc.* **2015**, *137*, 7015–7018.
- [20] A. Avellaneda, P. Valente, A. Burgun, J. D. Evans, A. W. Markwell-Heys, D. Rankine, D. J. Nielsen, M. R. Hill, C. J. Sumbly, C. J. Doonan, *Angew. Chem. Int. Ed.* **2013**, *52*, 3746–3749; *Angew. Chem.* **2013**, *125*, 3834–3837.
- [21] a) T. Mitra, K. E. Jelfs, M. Schmidtmann, A. Ahmed, S. Y. Chong, D. J. Adams, A. I. Cooper, *Nat. Chem.* **2013**, *5*, 276–281; b) M. Ortiz, S. Cho, J. Niklas, S. Kim, O. G. Poluektov, W. Zhang, G. Rumbles, J. Park, *J. Am. Chem. Soc.* **2017**, *139*, 4286–4289; c) L. Qiu, R. McCaffrey, Y. Jin, Y. Gong, Y. Hu, H. Sun, W. Park, W. Zhang, *Chem. Sci.* **2018**, *9*, 676–680; d) N. Sun, C. Wang, H. Wang, L. Yang, P. Jin, W. Zhang, J. Jiang, *Angew. Chem. Int. Ed.* **2019**, *58*, 18011–18016; *Angew. Chem.* **2019**, *131*, 18179–18184; e) X. Yu, B. Wang, Y. Kim, J. Park, S. Ghosh, B. Dhara, R. D. Mukhopadhyay, J. Koo, I. Kim, S. Kim, I.-C. Hwang, S. Seki, D. M. Guldi, M.-H. Baik, K. Kim, *J. Am. Chem. Soc.* **2020**, *142*, 12596–12601.
- [22] a) F. Beuerle, S. Klotzbach, A. Dhara, *Synlett* **2016**, *27*, 1133–1138; b) N. Schäfer, M. Bühler, L. Heyer, M. I. S. Röhr, F. Beuerle, *Chem. Eur. J.* **2021**, *27*, 6077–6085; c) K. Acharyya, P. S. Mukherjee, *Chem. Eur. J.* **2014**, *20*, 1646–1657; d) K. Acharyya, P. S. Mukherjee, *Chem. Commun.* **2015**, *51*, 4241–4244; e) K. Acharyya, S. Mukherjee, P. S. Mukherjee, *J. Am. Chem. Soc.* **2013**, *135*, 554–557; f) D. Beaudoin, F. Rominger, M. Mastalerz, *Angew. Chem. Int. Ed.* **2017**, *56*, 1244–1248; *Angew. Chem.* **2017**, *129*, 1264–1268; g) P. Wagner, F. Rominger, W.-S. Zhang, J. H. Gross, S. M. Elbert, R. R. Schröder, M. Mastalerz, *Angew. Chem. Int. Ed.* **2021**, *60*, 8896–8904; *Angew. Chem.* **2021**, *133*, 8978–8986; h) R. L. Greenaway, V. Santolini, A. Pulido, M. A. Little, B. M. Alston, M. E. Briggs, G. M. Day, A. I. Cooper, K. E. Jelfs, *Angew. Chem. Int. Ed.* **2019**, *58*, 16275–16281; *Angew. Chem.* **2019**, *131*, 16421–16427; i) V. Abet, F. T. Szczypiński, M. A. Little, V. Santolini, C. D. Jones, R. Evans, C. Wilson, X. Wu, M. F. Thorne, M. J. Bennisson, P. Cui, A. I. Cooper, K. E. Jelfs, A. G. Slater, *Angew. Chem. Int. Ed.* **2020**, *59*, 16755–16763; *Angew. Chem.* **2020**, *132*, 16898–16906; j) T. Jiao, G. Wu, L. Chen, C.-Y. Wang, H. Li, *J. Org. Chem.* **2018**, *83*, 12404–12410.
- [23] a) T. Hasell, X. Wu, J. T. A. Jones, J. Bacsá, A. Steiner, T. Mitra, A. Trewin, D. J. Adams, A. I. Cooper, *Nat. Chem.* **2010**, *2*, 750–755; b) G. Zhang, O. Presly, F. White, I. M. Oppel, M. Mastalerz, *Angew. Chem. Int. Ed.* **2014**, *53*, 5126–5130; *Angew. Chem.* **2014**, *126*, 5226–5230; c) Z. Sun, P. Li, S. Xu, Z.-Y. Li, Y. Nomura, Z. Li, X. Liu, S. Zhang, *J. Am. Chem. Soc.* **2020**, *142*, 10833–10840.
- [24] V. Leonhardt, S. Fimmel, A.-M. Krause, F. Beuerle, *Chem. Sci.* **2020**, *11*, 8409–8415.
- [25] M. Mastalerz, *Synlett* **2013**, *24*, 781–786.

- [26] a) A. F. Bushell, P. M. Budd, M. P. Attfield, J. T. A. Jones, T. Hasell, A. I. Cooper, P. Bernardo, F. Bazzarelli, G. Clarizia, J. C. Hansen, *Angew. Chem. Int. Ed.* **2013**, *52*, 1253–1256; *Angew. Chem.* **2013**, *125*, 1291–1294; b) J. D. Evans, D. M. Huang, M. R. Hill, C. J. Sumby, A. W. Thornton, C. J. Doonan, *J. Phys. Chem. C* **2014**, *118*, 1523–1529.
- [27] a) M. Brutschy, M. W. Schneider, M. Mastalerz, S. R. Waldvogel, *Adv. Mater.* **2012**, *24*, 6049–6052; b) M. Brutschy, M. W. Schneider, M. Mastalerz, S. R. Waldvogel, *Chem. Commun.* **2013**, *49*, 8398–8400.
- [28] A. W. Markwell-Heys, M. L. Schneider, J. M. L. Madridejos, G. F. Metha, W. M. Bloch, *Chem. Commun.* **2021**, *57*, 2915–2918.
- [29] T. Tozawa, J. T. A. Jones, S. I. Swamy, S. Jiang, D. J. Adams, S. Shakespeare, R. Clowes, D. Bradshaw, T. Hasell, S. Y. Chong, C. Tang, S. Thompson, J. Parker, A. Trewin, J. Bacsá, A. M. Z. Slawin, A. Steiner, A. I. Cooper, *Nat. Mater.* **2009**, *8*, 973.
- [30] a) E. O. Pyzer-Knapp, H. P. G. Thompson, F. Schiffmann, K. E. Jelfs, S. Y. Chong, M. A. Little, A. I. Cooper, G. M. Day, *Chem. Sci.* **2014**, *5*, 2235–2245; b) A. G. Slater, P. S. Reiss, A. Pulido, M. A. Little, D. L. Holden, L. Chen, S. Y. Chong, B. M. Alston, R. Clowes, M. Haranczyk, M. E. Briggs, T. Hasell, G. M. Day, A. I. Cooper, *ACS Cent. Sci.* **2017**, *3*, 734–742; c) A. Pulido, L. Chen, T. Kaczorowski, D. Holden, M. A. Little, S. Y. Chong, B. J. Slater, D. P. McMahon, B. Bonillo, C. J. Stackhouse, A. Stephenson, C. M. Kane, R. Clowes, T. Hasell, A. I. Cooper, G. M. Day, *Nature* **2017**, *543*, 657–664.
- [31] a) J. T. A. Jones, T. Hasell, X. Wu, J. Bacsá, K. E. Jelfs, M. Schmidtman, S. Y. Chong, D. J. Adams, A. Trewin, F. Schiffmann, F. Cora, B. Slater, A. Steiner, G. M. Day, A. I. Cooper, *Nature* **2011**, *474*, 367–371; b) T. Hasell, S. Y. Chong, K. E. Jelfs, D. J. Adams, A. I. Cooper, *J. Am. Chem. Soc.* **2012**, *134*, 588–598; c) T. Hasell, M. A. Little, S. Y. Chong, M. Schmidtman, M. E. Briggs, V. Santolini, K. E. Jelfs, A. I. Cooper, *Nanoscale* **2017**, *9*, 6783–6790; d) S. Tothadi, M. A. Little, T. Hasell, M. E. Briggs, S. Y. Chong, M. Liu, A. I. Cooper, *CrystEngComm* **2017**, *19*, 4933–4941; e) A. G. Slater, M. A. Little, A. Pulido, S. Y. Chong, D. Holden, L. Chen, C. Morgan, X. Wu, G. Cheng, R. Clowes, M. E. Briggs, T. Hasell, K. E. Jelfs, G. M. Day, A. I. Cooper, *Nat. Chem.* **2017**, *9*, 17–25.
- [32] a) T. Hasell, J. L. Culshaw, S. Y. Chong, M. Schmidtman, M. A. Little, K. E. Jelfs, E. O. Pyzer-Knapp, H. Shepherd, D. J. Adams, G. M. Day, A. I. Cooper, *J. Am. Chem. Soc.* **2014**, *136*, 1438–1448; b) M. A. Little, S. Y. Chong, M. Schmidtman, T. Hasell, A. I. Cooper, *Chem. Commun.* **2014**, *50*, 9465–9468.
- [33] a) L. J. Barbour, *Chem. Commun.* **2006**, 1163–1168; b) M. Mastalerz, *Chem. Eur. J.* **2012**, *18*, 10082–10091.
- [34] G. R. Desiraju, *Nat. Mater.* **2002**, *1*, 77–79.
- [35] a) J. D. Evans, D. M. Huang, M. R. Hill, C. J. Sumby, D. S. Sholl, A. W. Thornton, C. J. Doonan, *J. Phys. Chem. C* **2015**, *119*, 7746–7754; b) B. Teng, M. A. Little, T. Hasell, S. Y. Chong, K. E. Jelfs, R. Clowes, M. E. Briggs, A. I. Cooper, *Cryst. Growth Des.* **2019**, *19*, 3647–3651; c) M. W. Schneider, I. M. Oppel, A. Griffin, M. Mastalerz, *Angew. Chem. Int. Ed.* **2013**, *52*, 3611–3615; *Angew. Chem.* **2013**, *125*, 3699–3703; d) S. Hong, M. R. Rohman, J. Jia, Y. Kim, D. Moon, Y. Kim, Y. H. Ko, E. Lee, K. Kim, *Angew. Chem. Int. Ed.* **2015**, *54*, 13241–13244; *Angew. Chem.* **2015**, *127*, 13439–13442; e) H. Ding, Y. Yang, B. Li, F. Pan, G. Zhu, M. Zeller, D. Yuan, C. Wang, *Chem. Commun.* **2015**, *51*, 1976–1979; f) C. G. Bezzu, M. Helliwell, J. E. Warren, D. R. Allan, N. B. McKeown, *Science* **2010**, *327*, 1627–1630.
- [36] K. Su, W. Wang, S. Du, C. Ji, M. Zhou, D. Yuan, *J. Am. Chem. Soc.* **2020**, *142*, 18060–18072.
- [37] a) D. Kuck, A. Schuster, B. Ohlhorst, V. Sinnwell, A. de Meijere, *Angew. Chem. Int. Ed. Engl.* **1989**, *28*, 595–597; *Angew. Chem.* **1989**, *101*, 626–628; b) D. Kuck, *Chem. Rev.* **2006**, *106*, 4885–4925; c) D. Kuck, *Chem. Rec.* **2015**, *15*, 1075–1109; d) A. Dhara, F. Beuerle, *Synthesis* **2018**, *50*, 2867–2877.
- [38] a) T. Ben, S. Qiu, *CrystEngComm* **2013**, *15*, 17–26; b) S. Grosjean, Z. Hassan, C. Wöll, S. Bräse, *Eur. J. Org. Chem.* **2019**, 1446–1460.
- [39] Spartan'18, Wavefunction, Inc. Irvine, CA (USA).
- [40] The PyMOL Molecular Graphics System, Version 2.4.2 Schrödinger, LLC.
- [41] Deposition numbers 2064668 (**2-Me**), 2064669 (**2-Et**) and 2064670 (**2-Bu**) contain the supplementary crystallographic data for this paper. These data are provided free of charge by the joint Cambridge Crystallographic Data Centre and Fachinformationszentrum Karlsruhe Access Structures service.
- [42] A. Burkhardt, T. Pakendorf, B. Reime, J. Meyer, P. Fischer, N. Stübe, S. Panneerselvam, O. Lorbeer, K. Stachnik, M. Warmer, P. Rödig, D. Göries, A. Meents, *Eur. Phys. J. Plus* **2016**, *131*, 56.
- [43] G. M. Sheldrick, *Acta Crystallogr. Sect. A* **2015**, *71*, 3–8.
- [44] a) P. Van Der Sluis, A. L. Spek, *Acta Crystallogr. Sect. A* **1990**, *46*, 194–201; b) A. L. Spek, *Acta Crystallogr. Sect. D* **2009**, *65*, 148–155.
- [45] M. Thommes, K. Kaneko, A. V. Neimark, J. P. Olivier, F. Rodriguez-Reinoso, J. Rouquerol, K. S. W. Sing, *Pure Appl. Chem.* **2015**, *87*, 1051–1069.
- [46] BIOVIA, Dassault Systèmes, Materials Studio, Release 17.11.10.48, San Diego: Dassault Systèmes, 2017.
- [47] M. Liu, L. Zhang, M. A. Little, V. Kapil, M. Ceriotti, S. Yang, L. Ding, D. L. Holden, R. Balderas-Xicohténcatl, D. He, R. Clowes, S. Y. Chong, G. Schütz, L. Chen, M. Hirscher, A. I. Cooper, *Science* **2019**, *366*, 613–620.

Manuscript received: February 28, 2021

Revised manuscript received: April 23, 2021

Accepted manuscript online: April 27, 2021

Version of record online: May 26, 2021